ELSEVIER

Astroparticle Physics 7 (1997) 219–230

Astroparticle Physics

Study of the combined particle identification capability of a transition radiation detector and a silicon imaging calorimeter during the TS93 balloon flight

R. Bellotti [a], F. Cafagna [a], M. Castellano [a], M. Circella [a], G. De Cataldo [a], C. De Marzo [a], N. Giglietto [a], B. Marangelli [a], A. Rainò [a], P. Spinelli [a,*], M. Brancaccio [b], M. Grandi [b], P. Papini [b], A. Perego [b], S. Piccardi [b], P. Spillantini [b], G. Basini [c], M. Ricci [c], A. Codino [d], N. Finetti [d], C. Grimani [d], V. Bidoli [e], M. Candusso [e], M. Casolino [e], M.P. De Pascale [e], A. Morselli [e], P. Picozza [e], R. Sparvoli [e], F. Aversa [f], G. Barbiellini [f], M. Boezio [f], A. Colavita [f], F. Fratnik [f], P. Schiavon [f], A. Vacchi [f], N. Zampa [f], J.W. Mitchell [g], R.E. Streitmatter [g], R.L. Golden [h], S.J. Stochaj [h], M. Hof [i], W. Menn [i], M. Simon [i], S.A. Stephens [j]

[a] *Dipartimento di Fisica and Sezione I.N.F.N., Università di Bari, Italy*
[b] *Dipartimento di Fisica and Sezione I.N.F.N., Università di Firenze, Italy*
[c] *Laboratori Nazionali dell'I.N.F.N., Frascati, Italy*
[d] *Dipartimento di Fisica and Sezione I.N.F.N., Università di Perugia, Italy*
[e] *Dipartimento di Fisica and Sezione I.N.F.N., Università di "Tor Vergata", Roma, Italy*
[f] *Dipartimento di Fisica and Sezione I.N.F.N., Università di Trieste, Italy*
[g] *N.A.S.A. Goddard Space Flight Center, Greenbelt, MA, USA*
[h] *New Mexico State University, Las Cruces, USA*
[i] *Siegen University, Siegen, Germany*
[j] *Tata Institute of Fundamental Research, Bombay, India*

Received 3 November 1996; revised 2 March 1997; accepted 29 April 1997

Abstract

The WiZard Collaboration is involved in a program studying the antimatter components of the cosmic rays. A transition radiation detector and a silicon-tungsten calorimeter with imaging capabilities have been built as part of this program. We present the combined performance of these two detectors for positron identification during a balloon flight on September 8, 1993. The flight was dedicated to the measurement of the positron spectrum in the energy range 4–50 GeV and was launched from Ft. Sumner, New Mexico. © 1997 Elsevier Science B.V.

* Corresponding author.

PII S0927-6505(97)00027-3

1. Introduction

The WIZARD collaboration has performed an experiment—named TS93 [1]—to measure the spectrum of the positron component of cosmic rays in the energy interval 4–50 GeV. The low energy limit has been determined by the geomagnetic cutoff at the launch site (Ft. Sumner parallel, 34°N latitude) and the upper limit has been imposed by the 25 hours of exposure time. The experiment was flown on September 8th, 1993 at about 36 km of average altitude.

This measure is part of a larger program to study fluxes of both antiprotons in the 1–20 GeV energy range and positrons in the 4–50 GeV energy range, by different flights, with higher accuracy in particle identification with respect to past experiments [1]. The program deals with open questions in cosmic ray physics and particle astrophysics related to the origin of antiparticles, production and acceleration of particles, their propagation and confinement mechanisms inside the Galaxy.

The particular objective of the TS93 experiment was to measure the e^+/e^- ratio in the region of 10 GeV and above, that is in an energy interval where all the observations produced to date are affected by uncertainties connected with the subtraction of a significant background due to the high flux of protons respect to positrons.

The experimental situation on the ratio $R = N(e^+)/[N(e^+) + N(e^-)]$ is shown in Fig. 1 [2], where data from previous balloon flights are compared. Results obtained with the present experiment have been published separately [3].

A drawing of the experimental payload is shown in Fig. 2. A cosmic ray coming from outside the Earth crosses approximately 4.5 g/cm^2 of residual atmosphere before entering the payload. A superconducting magnet equipped with multiwire proportional chambers and drift chambers is used as a

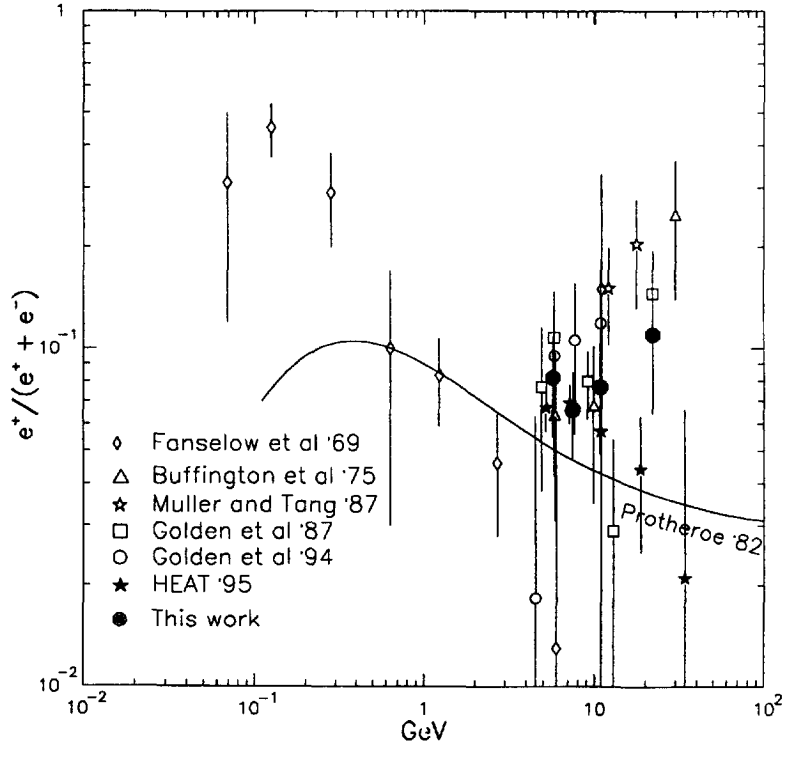

Fig. 1. Experimental situation on the positron data.

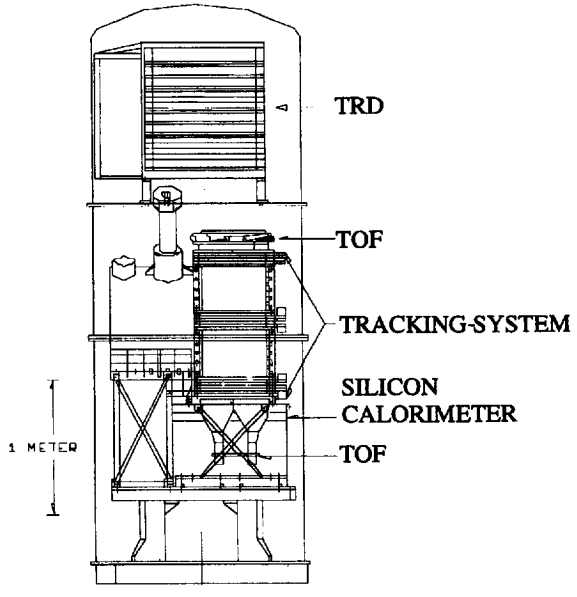

Fig. 2. Balloon flight complete detector housed in the container.

spectrometer [4,5]. A set of plastic scintillators, installed at the upper and lower extremes of the tracking system, provides both the trigger for the experiment and the time of flight (TOF) information with a resolution of 400 ps r.m.s. over 1.4 m of path; an energy loss (dE/dx) measurement over a total thickness of 2 cm of the two plastic scintillator layers is provided as well. The detectors used for positron identification in the TS93 flight are a transition radiation detector (TRD) and a silicon tungsten imaging calorimeter (Si–Cal). Since the e^+/p ratio is known to be in the range from 10^{-3} to 10^{-4}, we need to rely on an apparatus which has a probability to identify erroneously a proton as a positron of the order of 10^{-5} or less. For this purpose the Si–Cal was employed in conjunction with the TRD, requiring for both the devices a rejection factor against protons of the order of 10^{-3}. The rejection factor against hadrons can be defined either as:

$$R_{h/e} = e_h/e_e$$

where e_h, e_e are the efficiencies for hadrons and electrons respectively, and e_e usually is 90%; or as:

$$R'_{e/h} = e_e/e_h.$$

Sometimes the hadron contamination at 90% electron efficiency is also used as rejection factor indicator, which simply corresponds to e_h.

In this paper we describe the performances of the two detectors, both separately and combined. We will show that during the flight it has been possible to achieve an overall proton rejection factor R of the order 10^{-5}—namely $R' = 3 \times 10^4$—as required.

2. TRD general description

The transition radiation detector is placed on the top of the magnet spectrometer inside the balloon payload container, usually referred to as 'gondola', and has an active area of 76×80 cm^2, chosen to match at best the acceptance of the rest of the apparatus (Fig. 2). A detailed description of the detector has already been published in [6].

The TRD peculiar characteristics, common to other detectors that have been operated in similar experimental conditions, are the reduced weight (237 kg) and the limited electric power supplied (100 W for 2560 electronic channels); nevertheless its performances are equivalent to analogous devices working in accelerator experiments.

The detector consists of ten carbon fiber radiators each followed by a multiwire proportional chamber (MWPC) housed inside an aluminum box (Fig. 3). The total radiation and interaction lenghts are 0.13 X_0 and 0.05 λ_I respectively.

Each radiator consists of a light and stiff aluminum frame containing four polyethylene bags filled with carbon fiber segments, and it has overall dimensions of $80 \times 80 \times 5$ cm^3. The radiator density has been fixed to the optimal value of 0.060 g/cm^3. The first (top) TRD module has an additional identical radiator to get nearly the same radiation yield as the following ones. The same setup has been used in the prototype exposed to test beam and a similar one is generally used by many other authors, when space is available.

The proportional chambers have an active surface of 76×80 cm^2 and an anode–cathode gap fixed to 8 mm in our design. Each anode plane is equipped with 256 gold plated tungsten wires, 25 μm thick, stretched to a tension of 70 g with 3 mm spacing. In these conditions, at the typical operation high voltage (2.95 KV), no intermediate anode to cathode spacer is needed to prevent wire instabilities.

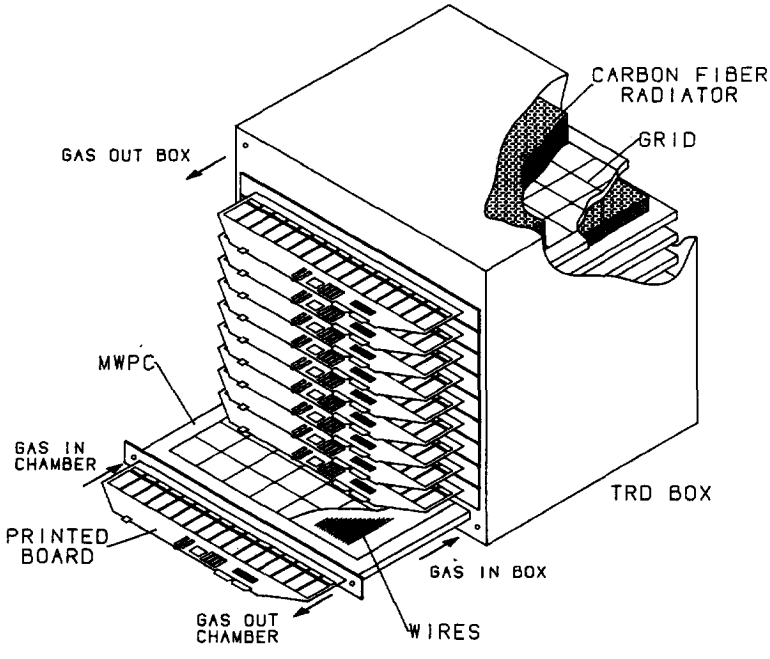

Fig. 3. TRD artist's view with inner chambers and radiators details.

No windows external to the cathode planes have been used in this chamber design. In order to prevent cathode plane deformations, due to possible unbalance of the chamber gas pressure with respect to the external one, the cathode foils have been reinforced externally by a set of thin fiber glass strips stretched across the external frames. With this solution the amount of material between the chamber gas volume and the radiator is quite negligible and, in addition, no electric field non-uniformities have been observed when the inner pressure is kept below 50 μbar above the outer pressure.

The chambers are filled with a xenon (80%)–methane (20%) mixture chosen to give optimal TR photon conversion with low δ-ray background production. With such a mixture the electron drift velocity results to be about 300 ns/cm at the operational high voltage supply.

The high voltage supplied is remote controlled and adjustable in steps of 1 V up to 5000 V. The adjustable voltage was used to correct the variations in operating temperature and pressure during the flight by monitoring the stability of the reference signal amplitude of the chambers produced by X-ray Fe^{55} sources.

The ten TRD modules are inserted in a light aluminum rack secured inside an aluminum box. This box, designed to withstand a 10 G shock, is sealed by a flange which allows only a short terminal part of the MWPC printed boards to come out just to be connected to the read-out electronics boards as shown in Fig. 3. The box ensures both mechanical stability and shock protection of the inner detector.

During the TRD operation the xenon–methane mixture in the chambers and the methane in the box are permanently flown. The two flows (about 20 l/h and 2 l/h respectively) are regulated by two electro-valves. A unit MKS 1250A remotely controls these valves by two pressure transducers in order to keep the differential pressure between the chamber and the box volume to 50 μbar, and between the box and the gas contained in the balloon payload to 20 μbar. The control unit compares the signal level (0–5 V) of the transducer to a reference voltage that can be set remotely by a DAC. This signal results to grow linearly with pressure in our range. In this way accurate planarity of cathode planes is ensured independently from pressure variations inside the payload container.

We have chosen to flow methane into the box in

order to have a limited X-ray absorption in the space before the cathodes and inside the radiators and also to limit the deterioration of the chamber gas mixture caused by the diffusion of the external gas through the mylar cathode planes.

3. TRD electronics description

Detection of transition radiation (TR) photons was based on the 'cluster counting' method first introduced by Fabjan et al. [7]. In this method, photoionization charge clusters are counted when the corresponding anode signal amplitudes overcome a given threshold. This solution was mainly suggested by the simplicity of the relative electronics, given the large number of channels involved, and by the possibility to easily turn to a design based on low power consumption components. An additional reason for the cluster counting choice was the well known stability of the rejection factor with respect to changes of the threshold set on the cluster amplitude [6,8] or to possible chamber signal amplitude variations (foreseen within a few tens of percent). This feature is very important in our experimental conditions because of the pressure and temperature changes inside the payload and on account of limitations on the flow of control signals.

The front-end and read out electronic components of each chamber are mounted on a single mother board directly connected to the anode plane printed board connectors (see Fig. 3). The read-out and control signal levels are loaded on a ribbon cable bus, common to all the chambers, which is connected to a CAMAC interface module. On the same electronic board, a gate signal from the trigger logic is distributed to each channel. The power supply is regulated on each board to ± 5 V.

In order to reduce the power consumption to about 40 mW/channel corresponding to an overall power of about 100 W, as assigned to the TRD during the flight, we have developed a new front-end electronic channel based on hybrid circuitry technology. The main interesting feature of the front end channel is the low power consumption, namely 35 mW with 50 MHz bandwidth.

The channels of each chamber are grouped into blocks of 16 on single cards mounted on the mother board by special connectors. The single channel consists of a hybrid circuit preamplifier and an amplifier–discriminator chain. The discriminator output is delayed by 110 ns and sent to an AND-gate in time with the external trigger gate G. This trigger signal is derived from the time of flight counters and is set to a width of 350 ns to fully account for the drift time of the clusters of electric charge, released by the TR photons, towards the anode wire. The pulses passing the AND-gate are counted by a 4 bit counter and transferred to the CAMAC interface module to be read out into the on line computer. All the components used immediately downstream the hybrid circuits are based on HCMOS family, to get both low power consumption and fast switching, in order to correctly count the cluster pulses.

The amplifier provides two outputs: one is sent to the discriminator; the other one is sent to a buffer stage and is used to monitor the gain stability of the chamber. In the chamber operation conditions discussed above, the pulse of an ionization cluster produced by a 5.9 keV X-ray has a nearly symmetric shape of 30 ns F.W.H.M. and amplitude of about 100 mV on a 50 W load. The overall double pulse resolution of the channel, which is very important for a correct cluster counting ability, has been measured by test signals of 10 ns width and was 25 ns.

4. Results of the TRD beam calibration

We have used a pion/electron beam, described previously in [6,8], to test a prototype of the TRD having the same parameters and equipped with the electronics described above. The beam momentum was varied from 1 to 5 GeV/c in steps of 1 GeV/c.

The threshold of the discriminator for cluster counting was set to a voltage level (80 mV) corresponding to a TR photon of about 5 keV, where the pion contamination at 90% electron efficiency reaches a broad minimum as already verified in [8]. All chambers were continuously calibrated during their operation by a Fe^{55} (5.9 KeV) and a Cd^{109} (22 keV) X-ray source. The resulting charge collected on any wire was linear with photon energy up to 22 KeV. At the high voltage used (2.95–3 kV) the gas gain was slightly above 10^4.

Additional tests were performed to study the chamber response with respect to variations in temperature and pressure as expected during the flight. The temperature has been varied from 17°C up to 40°C and the signal pulse height from the Fe^{55} source was measured. In order to keep constant the pulse height, the high voltage correction factor to be applied is on the average about -10 V/°C. The pressure dependence of the signal was also studied in the range 870–1000 mbar, yielding a correction ratio on the high voltage of about 12.5 V/mbar.

The pion contamination versus the electron efficiency was investigated for different analysis approaches. For the purpose four parametric procedures

1. counting of planes fired in the track,
2. counting of clusters in the track,
3. likelihood method,
4. geometric mean of the number of chambers fired (n_{ch}) and total clusters (n_{cl}), namely $g = [n_{ch} \cdot n_{cl}]^{1/2}$;

and a non-parametric procedure:

– neural network technique.

where implemented.

In the first procedure we analyzed the particle hit pattern in the ten chambers and for both kind of particles we counted the wire planes where at least one hit along the track is recorded. We then applied a variable cut on the two count distributions and calculated the pion contamination and relative electron acceptance.

In the second procedure we counted the hits belonging to the track only, although hits not farther than one wire from the track were also accepted. In this way most hits originated by δ-rays, ejected by the particle at large angles with respect to its trajectory, are disregarded. In the third case we used the same likelihood procedure introduced by Cherry [9] to distinguish different mass particles whose signals are pulse height analyzed. In the last case we simply calculated the geometric mean of the number of chambers fired and the total number of clusters detected along the track. We can see that this method gives much better results than the first two methods and it is equivalent to the third one but simpler to apply. In fact with this electronics we can achieve a pion contamination of about 2×10^{-3} at 90% electron acceptance beyond $\gamma = 6 \times 10^3$, ($R' = 500$) as we can notice in Fig. 4. Finally a careful multidimensional analysis has been carried out by a neural network (NN) based method. In this case we got a rejection factor still of the order of 2×10^{-3} at 90% pion acceptance, but sensibly lower than the previous methods while approaching to 100% acceptance [10,11]. For cross check reasons we have used the last two methods in this flight performance analysis

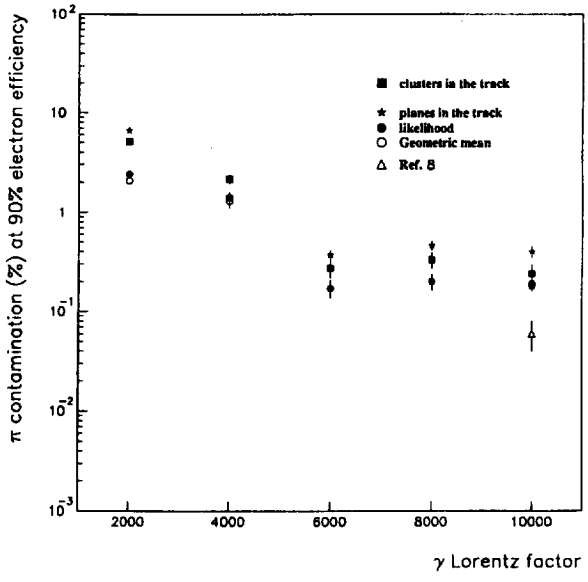

Fig. 4. Pion contamination versus particle Lorentz factor of the TRD.

5. Silicon-tungsten imaging calorimeter general description

The silicon tungsten detector (Si–Cal) developed for the TS93 flight (Fig. 2) has been configured to add three orders of magnitude in hadron rejection power to the rest of the spectrometer [12,13]. It acts as a high granularity track and shower imaging device. It allows to measure the shape and the energy left by developing showers as well as the shower starting point and the direction of the originating particle. All these features have been also combined with the specific requirements of low weight and low power consumption.

The complete device consists of five 'xy' layers of silicon detectors, interleaved with four planes of

tungsten 3.5 mm thick (1 X_0). A single sensitive layer is an array of 8×8 pair $(x-y)$ of detectors, each having a total area of 60×60 mm^2 and a thickness of 380 μm; their pitch is 3.6 mm (for a total of 16 strips per detector). The 'y' layers are mounted back to back with an on-line pin structure and perpendicular strips to give x and y coordinates. These pairs of detectors are held in a special package which allows a minimal dead area for the sensitive layer (5% of the total surface). The strips of each detector are daisy-chained longitudinally to form one strip 48 cm long; since the strip capacitance of each detector at full depletion is 70 pF, the total input capacitance to the preamplifier comes out to be 560 pF on the average. A multilayer board is used to patch all the detector and carries also the frontend electronics and the related wiring.

In order to be qualified for the balloon flight, the mechanical structure of the calorimeter has been designed to support 10 G vertically and 5 G horizontally. Moreover, the calorimeter has to hold the weight of the above tracking system and of part of the magnet; this requiring a solid and compact structure as less heavy as possible. The basic element of the internal mechanical structure is an anodised aluminum honeycomb base plate with four steel posts which follow the structure of the tracking system. A series of threaded columns, 5 mm diameter, welded on each side of the base plate allow the assembly of the silicon layers, the tungsten planes and the electronics. An internal top cover, made of Ergal (an aluminum alloy), tightly compresses the entire structure, thus preventing from any kind of oscillation and distributing the stresses over the four posts. The whole structure is sealed by an aluminum cover, 2 mm thick. It provides the termal insulation and the protection from light and dust. The environment is kept dry by a nitrogen flux.

A cooling device, a vacuum-proof stainless steel (1 mm thick) box containing 25 l of water, has been applied on the external side of the base plate, in order to keep the internal environment cooler than the payload, whose temperature varies from 10 to 38°C during the flight. The concept of this device is based on the evaporation of water in almost vacuum conditions (about 4 mbar at floating altitude); since the pressure inside the payload is mantained at 1 atm, the box is connected to the outside through a flexible pipeline. An electrovalve, normally open, placed along this line, prevents from any depressurizing hazard.

6. Silicon-tungsten imaging calorimeter electronics description

The design of a dedicated front-end electronics has been carried out in order to satisfy the requirements for a balloon flight. The basic unit consists of a 16 channel module providing the analog circuitry for the charge amplification and sample-and-hold of each channel, as well as the logic to drive the sample-and-hold itself and the multiplexed output. A post-amplifier is provided for each channel so that the signal may be read at two different amplification gains ($\times 1$ and $\times 16$), with the maximum output level (3.5 V) corresponding to 28 and 450 mip (minimum ionizing particle) respectively. The shaping time (7 μs) has been designed in order to optimize the signal-to-noise ratio.

The whole data acquisition system [14] has been integrated in the detector; it receives analogue signals from the pre-amplification modules, controls the digitization of the signals and performs a pedestal and zero suppression analysis, providing the resulting information to the flight control computer. Each plane has 16 programmable 12 bit ADCs, a 4 k-words double port memory (DPM) and one digital signal processor (DPS) acting both as a sequencer and as a CPU. In this way all the functions of each plane are executed in parallel. All DPSs are controlled by a master computer (GMX) that performs the execution of housekeeping tasks such as pedestal measurement, zero suppression threshold calculations and preamplifier linearity tests. The GMX writes the data on a dual port memory located in a CAMAC crate from which the flight control computer gathers the information to be transmitted to ground.

7. Calorimeter calibration results

An important step before proceeding to the analysis of the data collected by the Si–Cal is the calibra-

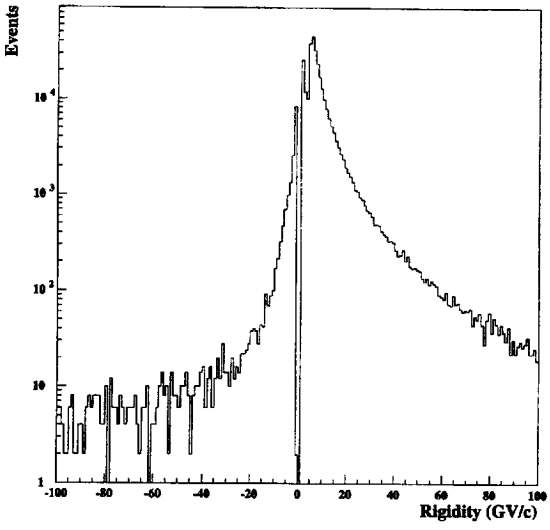

Fig. 5. Rigidity distribution of the in-flight detected particles as measured in the tracking system.

tion of its 1280 readout channels. In flight the calibration has been done using non interacting protons with rigidity $R > 4$ GV/c (where $R = p/Z$). These non interacting protons behave like minimum ionizing particles (mip). We fitted the ADC's distribution for each strip using a semi-gaussian function plus a Landau tail, thus obtaining the normalization coefficients for each channel.

During the flight we have observed good temporal stability of the strips and of the noise level, therefore the entire set of data has been normalized with the fitted coefficients. About 90% of the strips were fully active with a ratio of signal to noise for mip better than 15. Of the remaining strips, 5% gave no useful signal (detector or electronics failure); the others could be used in the case of high energy deposition only.

In Fig. 5 the rigidity distribution of the detected particles as measured in the tracking system is shown.

8. Particle identification performances during the flight

In the present analysis, flight data have been used to evaluate the signal/background discrimination capability of the detectors during the flight. TRD and Si–Cal flight performances in turn have been evaluated using a pure sample of real events selected by means of stringent cuts on the discriminating variables of the remaining detectors of the apparatus. In particular the TRD (Si–Cal) results have been worked out using data selected by the TOF, the spectrometer and the Si–Cal (TRD).

8.1. TRD performances

During the flight the payload pressure and temperature were carefully monitored to adjust accordingly the high voltage supply of the TRD chambers in order to keep the reference signal from the ^{55}Fe source to a value as stable as possible. The TRD particle identification capability has been measured using the information from the rest of the apparatus, and particularly the calorimeter. For this purpose we have selected a sample of electrons identified with high accuracy (the estimated contamination of this sample is 10^{-3}). The selection criteria were based on the negative curvature inside the magnetic field and on the electromagnetic shower developed in the calorimeter. Additional selection criteria were obtained by a Monte Carlo simulation, based on accelerator test data.

The response variation of the TRD to the electrons selected by the calorimeter has pointed that its performance have changed during the flight due to pressure and temperature variations, despite the implemented feedback on high voltage. We took into account these variations subdividing the data set into three more omogeneous sub-samples relative to different time intervals and defining the cuts selecting the electron sample at fixed acceptance. In Table 1, both proton contamination and rejection factor, obtained using the geometric mean procedure, are shown at an electron acceptance ranging from 50% to about 70%. Results obtained by means of neural network techniques can be found in [15,16].

In Fig. 6 we show the cluster number distributions for protons and electrons selected by the criteria described above. In Fig. 7 we show the average cluster count for the same particles at various γ Lorentz factors: in both cases the detector behaviour is consistent with the typical one published for traditional TRDs.

Table 1
Proton contamination and electron cut efficiency applied in different time intervals using the geometric mean g. The results for the cuts corresponding to about 50% and 70% electron efficiency are shown, respectively.

Time intervals (seconds)	Cuts	e^- efficiency	p^+ contamination	Rejection factor
$t < 45000$	$g \geq 3.25$	$46 \pm 2\%$	$0.29 \pm 0.02\%$	343 ± 39
$45000 \leq t < 85000$	$g \geq 3.25$	$54 \pm 2\%$	$0.49 \pm 0.02\%$	204 ± 14
$t \geq 85000$	$g \geq 4.25$	$47 \pm 2\%$	$0.17 \pm 0.03\%$	581 ± 103
All evts	(var cut)	$50 \pm 2\%$	$0.36 \pm 0.01\%$	279 ± 16
$t < 45000$	$g \geq 2.25$	$67 \pm 2\%$	$1.77 \pm 0.02\%$	56.5 ± 2.6
$45000 \leq t < 85000$	$g \geq 2.50$	$69 \pm 2\%$	$1.45 \pm 0.02\%$	69.0 ± 2.4
$t \geq 85000$	$g \geq 3.25$	$71 \pm 2\%$	$1.00 \pm 0.01\%$	100 ± 7.0
All evts	(var cut)	$69 \pm 2\%$	$1.45 \pm 0.02\%$	69.0 ± 2.0

From both analysis procedures we can realize that the rejection factor of the TRD is slightly worse than that obtained using the beam calibration data. This reduced performances can be attributed to different factors which showed up during the flight. To keep the gas gain to about 10^4 and to save at best the proportional behaviour of the chambers we did have not to exceed 3 kV in the H.V. supply, while the pressure ranged from 870 mbar to 1000 mbar and the temperature from 25°C to 38°C. Due to these pressure variations and the above H.V. limit, we had to run for one third of the flight with a discrimination threshold ranging from 4 to 7 KeV rather than the optimal 5 KeV, thus spoiling the rejection factor by a factor two.

Other factors contributing to reduce in flight the performances obtained in the test beam have been:

(1) to speed up the acquisition rate and to reduce the dead time due to the data transmission, we decided to read only the first five wires fired for each chamber. For this reason during the flight we lost useful information at 10% probability when

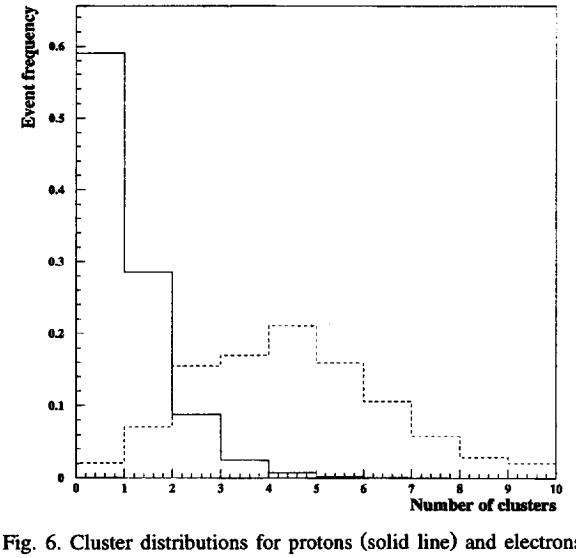

Fig. 6. Cluster distributions for protons (solid line) and electrons (dashed line) selected by the criteria described in the text.

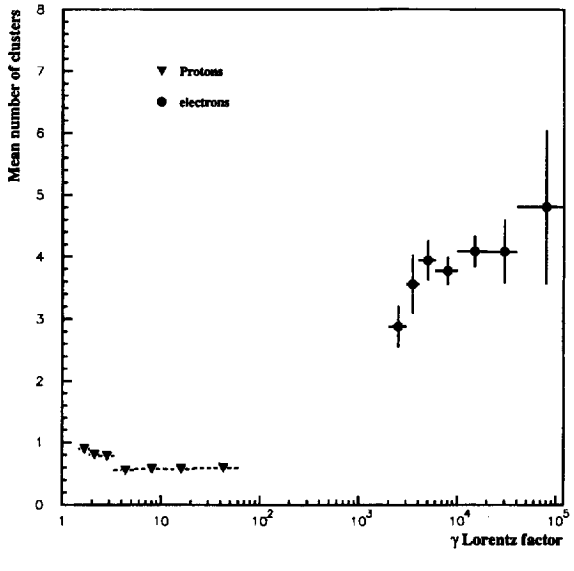

Fig. 7. Average cluster counts for electrons and protons in the TRD.

spurious signals were collected on these channels while the good ones were ignored since they occurred on the subsequent wires;

(2) during the flight, the top chamber manifested a quite noisy behaviour due to mechanical vibrations occurred to some wires, thus we excluded it from acquisition. In this way we had to run with nine out of ten chambers;

(3) to minimize spurious hits due to pick up e.m. noise from the other devices, just occurring at the beginning of the acquisition gate for the cluster counting, we had to delay it by about 30 ns, thus loosing about 12% of the useful counts.

In order to compare the in-flight rejection factor with that obtained with test beam data, we scaled down the calibration count distributions for pions and electrons accordingly to the reduced performances of the chamber data. The procedure was straightforward for all the cases described above, because we collected calibration data also in these anomalous conditions. For Case (1), in particular, we runned a Monte Carlo simulation describing the TRD behaviour after randomly cancelling each chamber response at the same rate as that of the occurring five wires fired (10%).

The rejection factor R against hadrons was 1.45×10^{-2}, at an acceptance level for electrons of 70%, in reasonable agreement with the flight results.

8.2. Silicon calorimeter performance

Real data sets of pure signal and background, selected by means of the TOF, the spectrometer and the TRD have been used to evaluate the performance of the Si–Cal during the flight. The discrimination of positrons from protons has been performed taking into account a set of 12 discriminating variables. They have been developed in order to describe the features of the e.m. cascade inside the detector as well as possible. Moreover they are built as being maximally invariant with respect to position within the detector, while retaining the largest amount of information contained in the pattern.

Besides some fundamental discriminating variables—as the total energy released by the showers in the silicon layers and the total number of hit strips in the calorimeter—other variables have been built in order to discriminate at best an electromagnetic from a hadronic shower. These variables describe some typical features characterizing the two kinds of cascades, both energetic and topological, due to the fact that, while an electron (or positron) induced shower is easy to describe, a hadronic cascade is much more complicated because of the variability of the hadron–nucleus interaction. All the adopted variables have been previously tested and optimimized on Monte Carlo simulated samples of events in order to obtain the most satisfactory results; the behaviour of these variables is clearly energy dependent.

One of the features to distinguish electronic versus hadronic showers is the trasversal development. While a hadronic shower has an unpredictable development, the transversal development of an e.m. shower is quite regular and is well described by the Molière theory, stating that 99% of an e.m. shower, at any energy, is contained in a cylinder of ratio $R = 3.5\ R_M$, where R_M is the Molière radius, whose value is fixed for each material and is 0.69 cm for tungsten. This well defined feature of the e.m. cascade has been used for constructing different variables useful for our analysis, like the ratio between the energy released in a cylinder of radius 1 R_M and the total energy deposited.

Another important difference between the two cascades is the symmetry. While an e.m. shower is rather symmetric, a hadronic one can have strange and different patterns in the detector.

Finally, the energy released by one of the secondaries in a hadronic shower can be very high—in case of pion, for instance—whereas secondaries in an e.m. shower are always electrons and positrons releasing relatively smaller energy deposits.

Applying one- and two-dimensional cuts (as a function of the particle rigidity) on these variables a proton rejection factor of 455 ± 21 at 0.79 ± 0.02 of efficiency is achieved, as it is described in [3]. These results permit a satisfactory signal identification in this experimental context. A different data analysis approach of the TS93 calorimeter data, based on artificial neural network techniques, can be found in [15,16].

Fig. 8a shows the reconstructed hit pattern of a positron candidate of 5 GeV energy as it appears in the TRD, tracking system and calorimeter respectively; Fig. 8b shows a proton candidate.

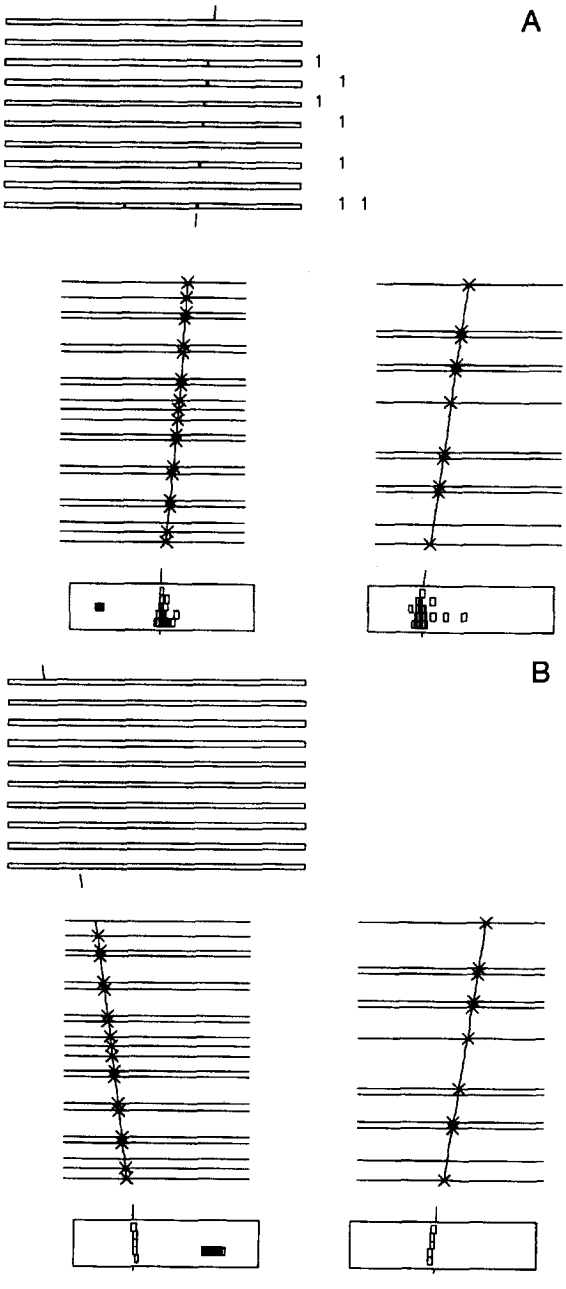

Fig. 8. Particle patterns in the TS93 apparatus: a) a positron candidate of 5 GeV energy; b) a proton candidate.

8.3. Overall rejection factor

Combining the TRD rejection factor (the lower part of Table 1) against protons—i.e. $R' = 69.0 \pm 2.0$ — with the corresponding rejection factor for the Si–Cal—i.e. $R' = 455 \pm 21$—we obtained the overall proton rejection factor of the entire apparatus $R' \approx 3 \times 10^4$, at 0.55 ± 0.02 of efficiency. With this identification performance we have been able to minimize the proton background in the positron sample as we have shown in [3].

9. Conclusions

The flight TS93 has collected almost 25 hours of useful data at float altitude. Using real data we determined the rejection factors of each ancillary TRD and Si–Cal detectors during the flight. An overall rejection factor of positrons against protons $R' = 3 \times 10^4$ (R of order 10^{-5}) was achieved, which is able in our experiment to separate unambiguously the positron signal from the large positive hadron background in the momentum range 4–50 GeV/c.

Acknowledgements

We acknowledge the valid contribution of Mr. M. Mongelli for the mechanical design of the TRD and of Mr. F.P. Ceglie and M. Franco to the mehanical set-up.

We are particularly grateful to Mr. E. Barbarito, Mr. A. Ceres, Mr. M. Perchiazzi, Mr. A. Sacchetti for the help in the electronic design, test, and on line set-up.

We thank Prof. H. Manon and Prof. M. Handlet of B.N.L. for the invaluable help in many fruitful discussions.

References

[1] R.L. Golden et al., Proposal to NASA NRA-92-OSSA-10.
[2] J.L. Fanselow et al., Ap. J. 158 (1969) 771; A. Buffington et al., Ap. J. 199 (1975) 669; R.L. Golden et al., Astr. Ap. 188 (1987) 145; D. Muller and K.K. Tang, Ap. J. 312 (1987) 183; R.L. Golden et al., Ap. J. 436 (1994) 769.
[3] R.L. Golden et al. (WIZARD-TS93 Coll.), Ap. J. 457 (1996) L103

[4] R.L. Golden et al., Nucl. Instr. Meth. A 306 (1991) 366.
[5] M. Hof et al., Nucl. Instr. Meth. A 345 (1994) 561.
[6] E. Barbarito et al., Nucl. Instr. Meth. A 357 (1995) 588.
[7] C.W. Fabjan et al., Nucl. Instr. Meth. 181 (1981) 119.
[8] E. Barbarito et al., Nucl. Instr. Meth. A 313 (1992) 295.
[9] M.L. Cherry et al., Nucl. Instr. Meth. 115 (1974) 141.
[10] R. Bellotti, M. Castellano, C. De Marzo, N. Giglietto, G. Pasquariello, P. Spinelli, Comp. Phys. Commun. 78 (1993) 17.
[11] R. Bellotti, M. Castellano, C. De Marzo, G. Pasquariello, G. Satalino, P. Spinelli, Nucl. Instr. Meth. A 350 (1994) 556.
[12] M. Bocciolini et al., Nucl. Instr. Meth. A 333 (1993) 560.
[13] M. Bocciolini et al., Nucl. Phys. 32 (1993) 77.
[14] F. Aversa et al., Nucl. Instr. Meth. A 334 (1993) 589.
[15] R. Bellotti et al., Proc. XXIV Int. Cosmic Ray Conf., Rome (1995) Vol. 3, p. 730.
[16] F. Aversa et al. (WIZARD-TS93 Coll.), Astropart. Phys. 5 (1996) 111.